The particle finite element method for transient granular material flow: modelling and validation

Simon Larsson[1] · Juan Manuel Rodríguez Prieto[1,2] · Gustaf Gustafsson[1] · Hans-Åke Häggblad[1] · Pär Jonsén[1]

Abstract

The prediction of transient granular material flow is of fundamental industrial importance. The potential of using numerical methods in system design for increasing the operating efficiency of industrial processes involving granular material flow is huge. In the present study, a numerical tool for modelling dense transient granular material flow is presented and validated against experiments. The granular materials are modelled as continuous materials using two different constitutive models. The choice of constitutive models is made with the aim to predict the mechanical behaviour of a granular material during the transition from stationary to flowing and back to stationary state. The particle finite element method (PFEM) is employed as a numerical tool to simulate the transient granular material flow. Use of the PFEM enables a robust treatment of large deformations and free surfaces. The fundamental problem of collapsing rectangular columns of granular material is studied experimentally employing a novel approach for in-plane velocity measurements by digital image correlation. The proposed numerical model is used to simulate the experimentally studied column collapses. The model prediction of the in-plane velocity field during the collapse agrees well with experiments.

Keywords Particle finite element method · Transient granular material flow · Constitutive modelling · Strain-rate-dependent strength · Digital image correlation

1 Introduction

A common aspect of various industrial processes and natural phenomena is the flow behaviour of dense granular materials. The lack of comprehensive theoretical models results in a low operating efficiency of industrial processes including dense granular material flow. A granular material is composed of a large number of individual particles of arbitrary size and shape. Although the individual particles may be of relatively simple geometrical shape, granular materials features a wide range of complex behaviours. The mechanical behaviour of a granular material is strongly dependent on the loading conditions. For quasi-static loading conditions, the behaviour is solid-like, while the behaviour of a flowing granular material typically is liquid-like [35]. The study of

granular material flow is of importance in many industries, such as the mining industry, the pharmaceutical industry and the agricultural industry. Numerical modelling and simulation provide insight into mechanisms of granular material flow that are difficult or impossible to study experimentally. High-quality numerical simulations of granular material flow are of great industrial interest, and such simulations require an adequate constitutive model and numerical method, but also high-accuracy experimental data.

Typically, granular material flow is modelled either at the particle scale, or at the continuum scale. The discrete element method (DEM), originally formulated by Cundall and Strack [15], is a method that has been widely used to model granular material flow in various industrial processes. In the DEM, each particle in the granular material mass is represented using a discrete particle. The motion of the discrete particles is determined by Newton's second law of motion, and the motion of the granular material mass is governed by the motion and interactions between the individual discrete particles. In the DEM, a small overlap is allowed at the contact between particles. The overlap is related to contact forces via a force–displacement law. The time integration of

✉ Simon Larsson
   simon.larsson@ltu.se

[1] Division of Mechanics of Solid Materials, Luleå University of Technology, SE-97187 Luleå, Sweden

[2] Mechanical Engineering Department, EAFIT University, Medellín, Colombia

Newton's equations typically proceeds in an explicit manner. Explicit integration requires that the time step size is kept low to ensure numerical stability. However, in some recent studies [66,71,72], the DEM has been implemented using implicit time integration schemes, allowing for much larger time steps. Implementations of the DEM commonly use spherical particles to represent non-spherical real granular particles. To accurately represent a non-spherical particle with a spherical particle requires careful selection of contact parameters. Attempts has also been made to use a multi-sphere approach to model non-spherical particles with the DEM [7]. A multi-sphere approach can be appropriate, but the authors still emphasize the difficulty and limitation of the method: the difficulty in calibrating micro-scale parameters for the DEM models. The DEM has traditionally been applied to model mainly frictional granular materials, but recently a growing interest in wet granular materials has stimulated the development of DEM models including capillary forces between particles [36]. When using the DEM, the computational cost increases with an increasing number of particles. Today, the availability of increasingly powerful computational resources has enabled simulation of large systems of granular materials, containing millions of particles [27]. However, the DEM is still impractical for the simulation of industrial size-scaled granular material flows, typically involving several billions of particles.

In a continuum approach, the granular mass is modelled as a continuum and its behaviour is predicted by fundamental laws of physics, namely the conservation of mass, momentum and energy. By this, the modelling of individual particles is avoided. Traditionally, when the continuum approach has been used for modelling of solid-like granular material behaviour, strain-rate-independent plasticity models, originating from Mohr–Coulomb plasticity, have been used, see e.g. [2,17,54,64]. In the literature [56], it has been shown that the mechanical behaviour of granular materials is strain rate independent in the quasi-static regime and strain rate dependent in the flow regime. In Andrade et al. [3], a strain-rate-dependent constitutive model for granular materials was formulated. The strain rate dependency was included by postulating a material strength that evolves with the strain rate.

When modelling fluid-like granular material behaviour, the focus has mainly been on the prediction of the steady-state flow regime. A visco-plastic rheology model, based on the use of a dimensionless inertia number, was used in [40,65] to model dense granular material flow. Promising results were obtained for flows on inclined planes and for the flow when a granular material was poured on top of a pile. However, the visco-plastic rheology approach is limited to flows where the inertial number is low, corresponding to relatively slow granular material flows. Furthermore, the solid-like granular material behaviour at quasi-static load-

ing cannot be captured, and no hysteresis is included. No inclusion of hysteresis means that an event where part of the granular material is static, while some other part of it is flowing, cannot be predicted correctly.

Modelling and simulation of the behaviour of granular materials with a continuum approach require, besides the selection of an adequate constitutive model, the choice of a robust and efficient numerical method. The finite element method (FEM) is a numerical method with a long tradition that has been used for numerical modelling in a wide range of technical fields [88]. When used with a Lagrangian description of motion, large deformations tend to severely distort the FE mesh, resulting in numerical difficulties. Thus, to use the FEM to model large deformation problems, some remedy for the mesh distortion is required. The FEM used with an Eulerian description of motion has been used to model granular material flow because it avoids mesh distortions at large deformation [23,42,83]. However, the FEM with an Eulerian description suffers from difficulties in predicting free surfaces and moving boundaries. The arbitrary Lagrangian–Eulerian (ALE) method attempts to overcome the inherent drawbacks of both Lagrangian and Eulerian descriptions. Drawing on the advantages of pure Lagrangian and pure Eulerian descriptions, the ALE method was used to model granular material flow in [13,14,78]. Advantages and disadvantages of using the FEM for the numerical simulation of forming processes involving large strains are discussed thoroughly in Rodríguez et al. [68].

There exist a number of particle methods within the continuum approach, and they provide an attractive alternative to the above-mentioned numerical methods, for the modelling of granular materials. Particle methods are commonly classified into two categories, particle methods that use a background mesh and particle methods that do not use a background mesh. One example of the latter is the smoothed particle hydrodynamics (SPH). The SPH was originally developed for the simulation of astrophysical problems [28,53]. The SPH is a Lagrangian mesh-free method, where the computational domain is represented by a set of particles. The particles also serve as the frame over which the field equations are approximated. In the SPH, no direct connectivity between particles exists. Thus, it can be used to treat problems involving large deformation, without suffering from the numerical difficulties inherent in mesh-based methods. The original SPH suffers from a number of drawbacks such as tensile instability, a lack of interpolation consistency, zero-energy modes, difficulties in handling essential boundary conditions and non-physical pressure oscillations. Furthermore, the SPH requires a homogeneous and smooth particle distribution to obtain stable and reliable results. This becomes particularly important in the evaluation of the pressure field. In recent versions of SPH, many of the inherent drawbacks of the original version have been addressed and

solved. Today, SPH is used for modelling in a wide range of engineering applications, including simulation of slope stability analysis and failure [6,58], and for the modelling of granular material flow [5,30,37–39,48,57,63].

The material point method (MPM) is a particle method that uses a background mesh. The MPM was developed by Sulsky et al. [75,76], and it is based on a combined Lagrangian–Eulerian description of motion. In the MPM, the state variables are traced on Lagrangian material points, while the equations of motion are integrated on a background computational mesh. The material points can be chosen independently of the mesh, and the connectivity between the material points changes dynamically during the simulation. In the MPM, each particle is assigned a fixed mass, which ensures mass conservation as long as the number of particles is kept constant throughout the simulation. Mass conservation is a strong advantage of the MPM, but since it is not easy to add or remove particles inside a given mass, the concentration of mass in localized areas might create problems. Since its original formulation, the MPM has become widely used for modelling in computational mechanics. Noteworthy publications include [10] where the MPM was used to treat localized large deformations for brittle failure and in [1] to model landslides using a Mohr–Coulomb yield criterion. Furthermore, the literature contains a number of studies where the MPM has been used to model granular material flow, for instance to model the granular material column collapse of frictional materials [20,24,55,74], cohesive–frictional materials [31] and silo discharge problems [80]. In a recent study by [32], a stabilized mixed implicit MPM was developed and used to model incompressible and compressible materials with a variety of plasticity laws. The MPM, combined with appropriate constitutive models, has been shown to adequately predict granular material flow at varying flow conditions.

The particle finite element method (PFEM) is another mesh-based particle method, and it is a Lagrangian particle method based on the FEM. The PFEM was initially developed for solving fluid dynamics problems in the context of fluid–structure interaction and free-surface flow [33,34,60]. The first extension of the PFEM to solid mechanics applications was made by Oliver et al. [59]. Recently, the flexibility and robustness of the PFEM have been demonstrated in a variety of engineering applications such as modelling of water waves generated by landslides [11,70], modelling rapid landslide run-outs with a Drucker–Prager model cast as a Bingham, non-Newtonian fluid model [12] and modelling of failure of rockfill dams with a Mohr–Coulomb model in a non-Newtonian Bingham form [46]. Furthermore, the PFEM has been used to model a variety of granular material flow problems, see e.g. [9,16,45,86]. In the PFEM, a Lagrangian description of motion is used for the nodes in a finite element mesh. The nodes are considered as free particles that are allowed to separate from the domain they originally are a part of. A cloud of particles is used to identify the computational domain, and a finite element discretization is utilized to advance the solution by a time increment. The particles contain all properties and variables, and the values of those are projected onto the mesh at each time increment, where the necessary equations are solved. The PFEM predicts a smooth pressure field, and the non-physical pressure oscillations typical for the SPH method are avoided. One advantage of the PFEM compared to the MPM is that in the PFEM it is possible to add or remove particles during the simulation; thus, concentration of mass in localized areas can be avoided.

If a numerical model is to be used for industrial decision-making, it needs to produce trustworthy results. Here, validation against experimental observations is of major importance. The continued development of numerical methods for modelling granular materials requires improved experimental methods that can provide high-accuracy results for model calibration and validation. Experimental insight into the flow dynamics can be obtained through in-plane velocity measurement, and such measurements are very useful for validation of numerical models. The introduction of digital photography has led to the development of optical experimental techniques such as digital particle image velocimetry (DPIV) [81]. In DPIV, a cross-correlation method is applied to a series of digital images to obtain the in-plane velocity field. DPIV was applied by [73] for field measurements of granular material flow during the discharge from plane hoppers. Digital image correlation (DIC) is an optical experimental technique that has been used extensively for the displacement and strain field measurement of materials subjected to large strains [41,62]. The DIC technique is based on the comparison of a series of digital photographs of a specimen surface recorded during deformation. Similar to the DPIV technique, a cross-correlation procedure is applied to determine the in-plane displacement field.

The collapse of granular material columns is an experimental set-up that has received much attention in recent years. The simplicity of the set-up and the ability to use it to study complex granular material flow phenomena have made the column collapse popular in the field of granular material flow. The set-up was popularized by [43] and [51] where cylindrical columns producing axisymmetric collapses were used. Their work revealed that the flow dynamics and deposit morphology were primarily dependent on the initial aspect ratio between the height and radius of the columns. Non-intrusive measurements of the deposit morphology using a laser scanner equipment were presented in [79]. In [85], particle tracking velocimetry was used to obtain in-plane velocity measurements of collapsing granular columns. In [47], the DIC technique was used to study and characterize granular material flow through field measurements.

The aim of the present study was to obtain a robust numerical tool for the simulation of granular material flow at dissimilar flow conditions. Transient granular material flow was modelled by the PFEM and a novel constitutive model where the internal friction of the granular material evolves with strain rate. To assess the capability of the proposed modelling framework, a set of numerical simulations of the fundamental problem of collapsing rectangular columns of granular material were performed. An extensive experimental investigation of the column collapse problem was performed where a novel experimental technique based on DIC was applied to quantify the flow dynamics in the form of in-plane velocity measurements. The proposed numerical model was validated by comparing results from the simulations with experimental measurements.

2 Materials and experimental study

In the present study, the flow dynamics of two granular materials was investigated experimentally. The main purpose of the experimental study was to obtain qualitative and quantitative measures of the flow of the granular materials, to be used for the calibration and validation of the proposed numerical model.

2.1 Materials

In the present study, two granular materials with very different properties were investigated. The first granular material was a potassium chloride (KCl) fertilizer, commonly known as muriate of potash (MOP). MOP denotes mixtures of KCl, at 95% or greater purity, and NaCl, which are adequate for agricultural use [77]. The particle size for the granular MOP was in the range of 2.0–4.0 mm, the particle shape was angular, the particle density was 1.99 g/cm^3, and the bulk density was 1.00 g/cm^3. The second granular material was a sintered aluminium oxide (Al$_2$O$_3$) used as a grinding media in liquid fine grinding in stirred media mills. The particle shape of the Al$_2$O$_3$ was spherical, and the particle size was in the range 1.2–2.0 mm. The particle density was 3.41 g/cm^3, and the bulk density was 2.13 g/cm^3. Optical light microscope images of the two granular materials are shown in Fig. 1, and it is observed that the granular materials have very different particle shapes. The particle shape of a granular material affects the internal angle of friction, which in turn affects its flowability. It has been shown [4,82] that particles with fairly spherical shape have a significantly lower internal angle of friction compared to that of particles with an angular and rough shape. In the present study, two granular materials with different particle shapes were chosen. The Al$_2$O$_3$ consists of spherical particles and the KCl with angular and rough particles. This choice was made deliberately
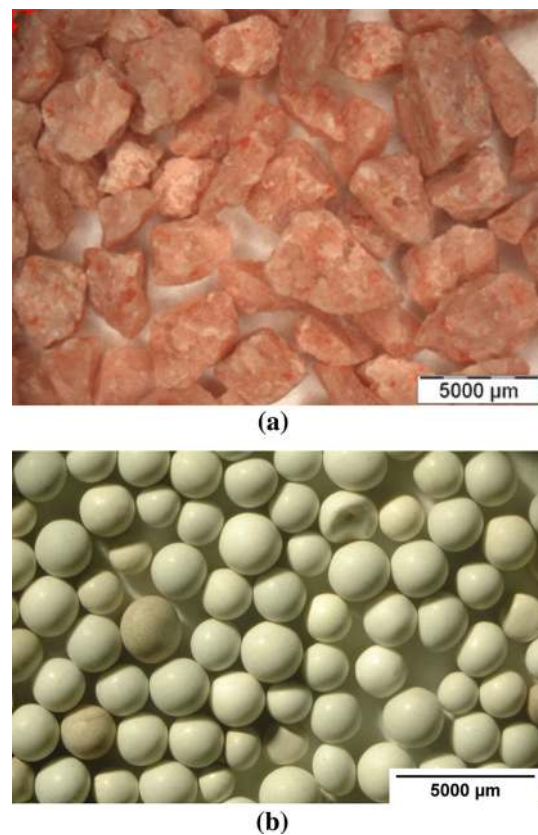
**Fig. 1** Optical light microscope images of (**a**) granular potassium chloride (KCl) fertilizer and (**b**) sintered aluminium oxide (Al$_2$O$_3$) grinding media

to investigate the ability of the proposed numerical model to represent granular materials with very different properties and bulk flow characteristics. Furthermore, an objective of the present study was to evaluate the performance of the proposed optical experimental technique for granular materials with different properties. Thus, this choice of granular materials was considered adequate by the authors.

2.2 Experimental set-up and procedure

The study of the transient material flows that occur during the collapse of columns of granular materials has been the focus in a number of studies. The collapse of axisymmetric granular material columns was studied experimentally in [43,51]. The rectangular channel column collapse was studied in [4,52]. The granular column collapse problem includes the kinematics of granular materials on different stages. Initially, the material is at rest in its container, and it then undergoes acceleration during the collapse and deceleration when the material comes to rest. Thus, the granular material column collapse experiment provides a good foundation for evaluating a numerical model of transient granular material flows. The experiments carried out in the present study constitute

Fig. 2 Schematic of the experimental set-up used for the granular material column collapse experiments
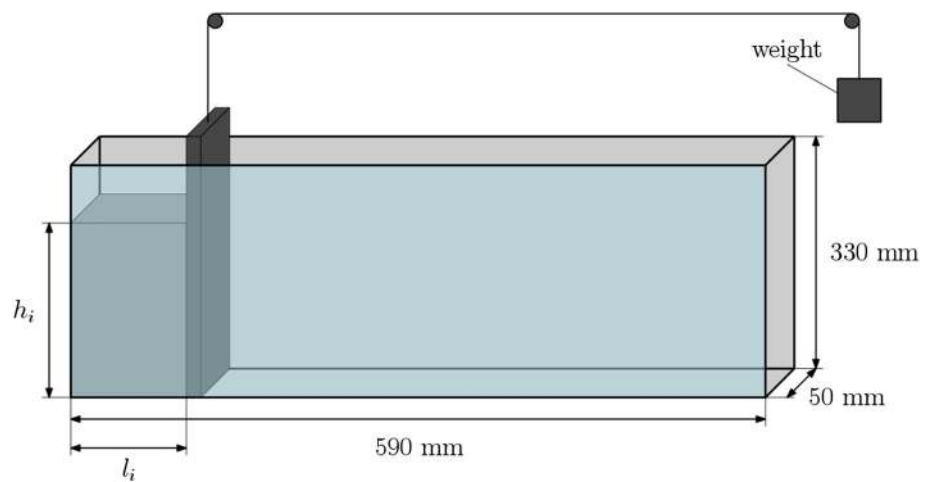
a complement to the experimental results found in the literature, especially concerning the optical measurements of the in-plane velocity field which are rarely found in previous studies.

An illustrative drawing of the experimental set-up used in the present study is shown in Fig. 2. The experimental set-up was designed as a 50-mm-wide, 590-mm-long and 230-mm-high closed rectangular channel. The front panel was made of hardened glass with a thickness of 4 mm. The other panels of the channel were made of steel with a thickness of 6 mm. The bottom of the channel was open, allowing it to be placed on surfaces made of different materials, with different surface properties. For all experiments in the present study, a smooth and horizontal bottom surface made of steel was used. A 6-mm-thick steel door was used to confine the granular materials in a reservoir prior to the collapse. The position of the door could be varied, enabling the study of a wide range of initial shapes of the granular mass. The design of the experimental set-up used in the present study was based on the set-ups used for rectangular channel column collapse experiments in [4,44].

The experimental procedure consisted in an initial positioning of the door and thus selecting a length l_i of the reservoir. The reservoir was then partly filled by carefully pouring a granular material mass to a height h_i. Thus, forming a rectangular column of granular material with a length of l_i, a height of h_i and a width of 50 mm. The top surface of the granular material was evened out by hand. The door was then quickly removed vertically via a weight, rope and pulley system (Fig. 2). The use of a weight, rope and pulley system made it possible to remove the door in a reproducible manner, keeping the vertical speed of the door constant at approximately 1.5 m/s for all the experiments. When the door was removed, the granular mass collapsed under the influence of gravity and spread horizontally in the channel until it came to a rest, forming a deposit profile. A conceptual initial set-up and final deposit profile are shown in Fig. 3.
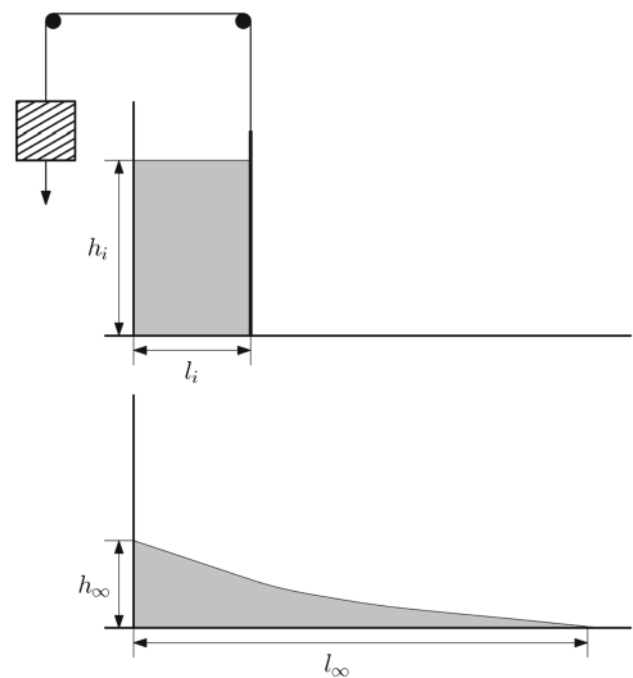
Fig. 3 Illustration of the initial set-up and the final deposit profile for the column collapse experiment

The ratio between the initial height h_i and length l_i was used to express the aspect ratio $a_i = h_i/l_i$ of the granular mass. The aspect ratio was varied by either using different amounts of granular material for a fixed door position and thus varying h_i, or by re-positioning the door and thus varying l_i. This procedure enabled the investigation of the collapse of columns of different masses but with the same aspect ratio. In total, 17 experiments were carried out for each granular material and the experimental parameters are presented in Table 1. Since all possible combinations of experimental parameters would result in a huge test matrix, the choice of h_i and l_i was made arbitrarily with the aim to cover the span of aspect ratios given in Table 1.

Table 1 Initial length l_i and height h_i, aspect ratio $a_i = h_i/l_i$ and mass in the series of column collapse experiments for KCl and Al_2O_3

Material	KCl				Al_2O_3			
Test	l_i [mm]	h_i [mm]	a_i	$Mass$[g]	l_i [mm]	h_i [mm]	a_i	Mass [g]
1	100	73	0.73	400	99	74	0.75	800
2	59	127	2.15	400	59	127	2.15	800
3	39	200	5.13	418	39	192	4.92	800
4	30	157	5.23	250	30	132	4.40	400
5	60	95	1.58	300	60	83	1.38	500
6	10	96	9.60	44	90	124	1.38	1166
7	100	83	0.83	440	10	97	9.70	96
8	50	152	3.04	400	110	66	0.60	750
9	30	92	3.07	148	40	98	2.45	400
10	50	104	2.08	270	20	49	2.45	96
11	20	124	6.20	130	30	98	3.27	300
12	10	63	6.30	33	20	121	6.05	250
13	20	158	7.90	165	10	60	5.95	58
14	20	169	8.45	180	20	151	7.55	300
15	60	61	1.02	190	20	161	8.05	330
16	90	107	1.19	510	10	81	8.05	81
17	40	162	4.05	340	70	70	1.00	500
18[a]	72	60	0.83	230	80	48	0.60	400
19[a]	22	115	5.23	130	21	92	4.38	200

[a]Tests recorded with the high-speed camera and processed using digital image correlation

The experiments were recorded with a high-speed digital camera. A MATLAB script was used to process the digital images to extract the final height h_∞, the final length l_∞ and the granular material deposit profile. For the KCl, l_∞ was defined as the horizontal position where the grains remained in contact with the rest of the granular mass. Thus, individual grains that had separated from the mass were not considered. For the Al_2O_3, l_∞ was defined as the horizontal position where the granular material layer ceased to have at least two grains in thickness. Furthermore, the digital images were processed using a commercial digital image correlation (DIC) software [29]. The methodology described in [47] was used to obtain the in-plane velocity field. In short, the DIC technique is based on the comparison of a series of digital images that are divided into overlapping sub-images. The in-plane velocity field is determined by applying a cross-correlation algorithm, which requires that the object to be traced is covered with a random surface pattern. The correlation algorithm is then able to trace the motion of the sub-images, and thus, the velocity field can be obtained. The granular materials that were used in the present study form a natural random surface pattern, and with a sufficient surface texture, the DIC technique could be used to obtain the in-plane velocity field. A more detailed description of the DIC and its application to quantify granular material flows can be found in [47].

2.3 Data acquisition

To record the experiments, a Redlake MotionPro X3 high-speed digital camera was used. During the recording, the granular materials were illuminated using two Dedocool floodlights equipped with 250 W lamps. The experiments were recorded with the high-speed camera set to capture 1000 images per second, at a resolution of 1280×720 pixels and with a shutter speed of 0.25 ms.

3 Numerical modelling and simulation

A granular material is a discrete media. However, in the present study the modelling of granular materials was based on the assumption that a granular material can be represented as a continuous media.

The assumption of using a continuum representation of discrete media is valid as long as the particles are much smaller than the smallest characteristic dimension of the process considered [21]. In the present study, two-dimensional computational domains were used to represent the granular materials. The PFEM, implemented in a MATLAB program, was used, and the granular materials were modelled using two different constitutive models.

3.1 Governing equations

The balance of linear momentum can be expressed in a Lagrangian description as

$$\rho \frac{Dv_i}{Dt} - \frac{\partial \sigma_{ij}}{\partial x_j} - b_i = 0, \tag{1}$$

where v_i and b_i are the velocity and body force components, ρ is the density, x_j are the material point positions, σ_{ij} is the Cauchy stress tensor and $\frac{Dv_i}{Dt}$ is the material derivative of the velocity field

$$\frac{Dv_i}{Dt} = \frac{\partial v_i}{\partial t} + v_j \frac{\partial v_i}{\partial x_j}. \tag{2}$$

The Cauchy stress tensor can be split into a mean stress component $\sigma_0 = \frac{1}{3} tr(\sigma_{ij})$ and a deviatoric component s_{ij} according to

$$\sigma_{ij} = s_{ij} + \sigma_0 \delta_{ij}, \tag{3}$$

where δ_{ij} is the Kronecker delta. Furthermore, it is assumed that the mass of a continuum body is conserved and that it is a continuous function of volume. The conservation of mass can be stated as

$$-\frac{1}{\kappa} \frac{D\sigma_0}{Dt} + \varepsilon_V = 0, \tag{4}$$

where κ is the elastic bulk modulus, $\frac{D\sigma_0}{Dt}$ is the material derivative of the mean stress and ε_V is the volumetric strain rate. The volumetric strain rate is defined as the trace of the rate of deformation tensor d_{ij}, which is given by

$$d_{ij} = \frac{1}{2} \left(\frac{\partial v_i}{\partial x_j} + \frac{\partial v_j}{\partial x_i} \right). \tag{5}$$

3.2 Constitutive models

Modelling a granular material as a continuum requires a constitutive model where the stresses in the material are related to some measure of deformation. Constitutive models may be dependent or independent of the strain rate, and in the present study, two strain-rate- dependent constitutive models were evaluated and compared.

3.2.1 Flow formulation

The first constitutive model is based on a constitutive relation for the flow of plastic and visco-plastic solids. It was originally outlined in [87] and was specialized in [8] to a Drucker–Prager yield surface [19], with a non-associated flow rule.

For large deformation, under plastic or visco-plastic conditions, elastic deformations can be neglected. A constitutive model linking the stresses and strain rates, where the viscosity is dependent on the current strain rates, can be formulated using the analogy with a viscous non-Newtonian incompressible fluid. The constitutive relation for an incompressible viscous fluid can be expressed as

$$\sigma_{ij} = \sigma_0 \delta_{ij} + 2\mu \dot{\varepsilon}_{ij}, \tag{6}$$

where μ is the viscosity and $\dot{\varepsilon}_{ij}$ is the strain rate tensor. Equation (6) can be rewritten using the split of the Cauchy stress tensor from Eq. (3)

$$\dot{\varepsilon}_{ij} = \frac{1}{2\mu} s_{ij}, \tag{7}$$

and following the definition of Perzyna non-associated viscoplasticity [69], Eq. (7) can be written as

$$\dot{\varepsilon}_{ij} = \frac{1}{\mu_p} \langle F \rangle \frac{\partial G}{\partial \sigma_{ij}}, \tag{8}$$

where μ_p is a 'pseudo-viscosity', $F = F(\sigma_{ij}) = 0$ is a plastic yield surface and $G = G(\sigma_{ij})$ is a plastic potential function. The use of Macaulay brackets in Eq. (8) means that $\langle F \rangle = F$ if $F > 0$ and $\langle F \rangle = 0$ if $F \leq 0$, thus ensuring no development of plastic flow if the stress state is inside the yield surface. If the viscosity parameter $\mu_p \to 0$, it implies that $\langle F \rangle \to 0$ in order for $\dot{\varepsilon}_{ij}$ to be a finite quantity. Thus, $\dot{\varepsilon}_{ij} \to \dot{\lambda} \partial G / \partial \sigma_{ij}$, where $\dot{\lambda}$ is the plastic multiplier. In other words, the visco-plastic relation in Eq. (8) reduces to rate independent plasticity theory when $\mu_p \to 0$.

Cante et al. [8] specialized the Perzyna relationship to the Drucker–Prager yield surface (Fig. 4), which has the following functional form

$$F = \sqrt{\frac{3}{2}} ||s_{ij}|| + b_1 \sigma_0 - b_2. \tag{9}$$

The parameter b_1 controls the influence of the mean stress on the yield limit, and it can be interpreted as the internal coefficient of friction of a granular material. The parameter b_2 corresponds to the yield strength of the material under pure shear, and in the context of granular materials, it can be interpreted as the granular material cohesion.

In the present study, the flow rule assigned to the Drucker–Prager yield surface is non-associated and consists of a purely deviatoric strain rate, and it can be expressed as

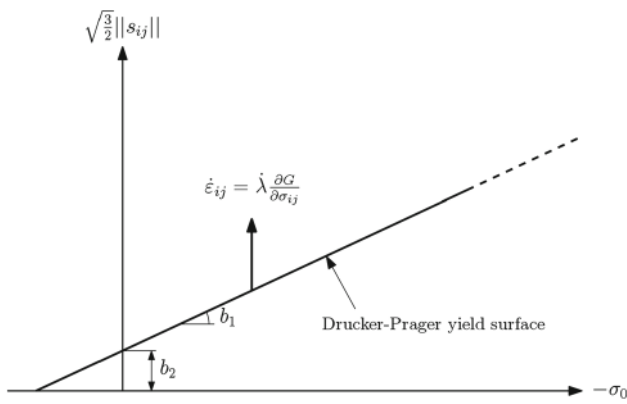$$\frac{\partial G}{\partial \sigma_{ij}} = s_{ij}. \tag{10}$$

Fig. 4 Drucker–Prager yield surface with a non-associated flow rule

The material flows at $F \geq 0$ and from Eqs. (8) to (10) the following expression can be obtained

$$6\dot{\bar{\varepsilon}}_{ij}\mu^2 + 2\mu(b_1\sigma_0 - b_2) - \bar{\mu} = 0, \tag{11}$$

where $\dot{\bar{\varepsilon}}_{ij} = \sqrt{\frac{2}{3}}||dev(\dot{\varepsilon}_{ij})||$ is the effective strain rate. For ideal plasticity, $\bar{\mu} \to 0$ and the viscosity can be written as

$$\mu = \frac{b_2 - b_1\sigma_0}{3\dot{\bar{\varepsilon}}_{ij}}. \tag{12}$$

Thus, a relationship between the deviatoric stresses and the strain rate has been obtained. Using the above results, this expression can be written in its final form as

$$s_{ij} = 2\mu\dot{\varepsilon}_{ij}. \tag{13}$$

3.2.2 Flow formulation with strain-rate-dependent residual strength

The second constitutive model used in the present study is based on a strain-rate-dependent plasticity model introduced in [3]. Considering the Drucker–Prager yield surface outlined in the previous section, the parameter b_1 is interpreted as the frictional resistance of the granular material. Andrade et al. [3] proposed a frictional resistance that is dependent on the dilatancy β and on a residual resistance $\bar{\mu}$

$$b_1 = \beta + \bar{\mu}. \tag{14}$$

The dilatancy is considered to be a function of the deviatoric shear strain ε_s, and its evolution is given by

$$\beta(\varepsilon_s) = \beta^* \frac{\varepsilon_s}{\varepsilon_s^*} \exp\left(1 - \frac{\varepsilon_s}{\varepsilon_s^*}\right), \tag{15}$$

where β^* is the maximum dilatancy and ε_s^* is the corresponding deviatoric shear strain. Following the form outlined in

[40], the evolution of the residual resistance is a function of the deviatoric shear strain rate $\dot{\varepsilon}_s$, and it is given by

$$\bar{\mu}(\dot{\varepsilon}_s) = \bar{\mu}_l + \frac{\bar{\mu}_u - \bar{\mu}_l}{1 + \dot{\varepsilon}_s^*/\dot{\varepsilon}_s}, \tag{16}$$

where $\bar{\mu}_l$ and $\bar{\mu}_u$ are the lower and upper bounds for the residual resistance, respectively. The lower and upper bounds are represented by $\dot{\varepsilon}_s \to 0$ and $\dot{\varepsilon}_s \to \infty$, respectively. The parameter $\dot{\varepsilon}_s^*$ is a characteristic deviatoric shear strain rate at which the residual resistance is $\bar{\mu} = 1/2(\bar{\mu}_l + \bar{\mu}_u)$. Thus, the frictional resistance b_1 is dependent on both the deviatoric shear strain and the deviatoric shear strain rate. The evolution of the frictional resistance is given by

$$b_1(\varepsilon_s, \dot{\varepsilon}_s) = \beta(\varepsilon_s) + \bar{\mu}(\dot{\varepsilon}_s). \tag{17}$$

The role of the dilatancy is to couple the deviatoric and volumetric components of deformation, and it describes the volume change of a material under shear deformation. The dilatancy is important for the mechanical behaviour of granular materials at quasi-static loading. It is in contrast to other materials, such as metals which are non-dilative. Dilatancy is important for granular materials in the solid-like state, but it can be neglected in the fluid-like state. In most granular material flows, the variation of the volumetric fraction is small [25], and if the granular material is considered as incompressible, the dilatancy and frictional equations are decoupled. Thus, the incompressible assumption greatly simplifies the constitutive model. In the present study, the granular materials were modelled as quasi-incompressible. Thus, the effect of the dilatancy was not included and the evolution of the frictional resistance is given by
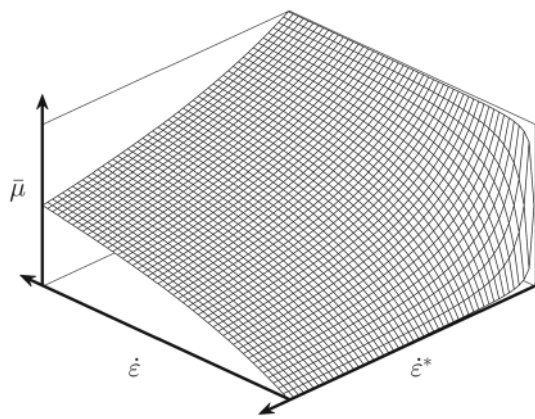
$$b_1(\dot{\varepsilon}_s) = \bar{\mu}(\dot{\varepsilon}_s). \tag{18}$$

The conceptual evolution of the residual strength as a function of $\dot{\varepsilon}_s$ and $\dot{\varepsilon}_s^*$ is shown in Fig. 5.

3.3 The particle finite element method

The PFEM is a particle-based numerical method where a background mesh is used and on which the FEM is used to solve the governing equations. The PFEM is founded upon modelling using an updated Lagrangian formulation. In the updated Lagrangian formulation, the equations are formulated in the current configuration, and the variables are assumed to be known at the last calculated configuration, at time t. The new variables are sought at the updated configuration, at time $t + \Delta t$. As outlined in [67], the PFEM can be divided into the following basic steps:
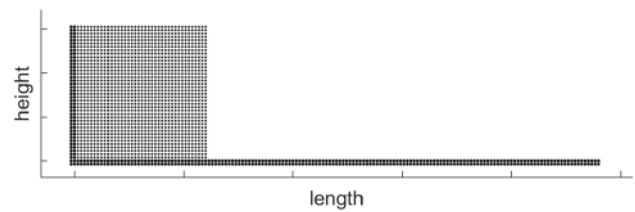
Fig. 5 Evolution of the residual strength $\bar{\mu}$ as a function of the deviatoric strain rate $\dot{\varepsilon}$ and the characteristic deviatoric strain rate $\dot{\varepsilon}_s^*$


Fig. 6 Conceptual illustration of the particle discretization of the domain in the two-dimensional plane deformation column collapse simulation. The initial particle disposition is regular and rectangular. In the figure, the fixed particles used to represent the bottom surface and left wall are shown in a darker shade

1. The computational domain is defined by a set of particles of infinitesimal size.
2. A finite element mesh is generated, using the set of particles as nodes. The finite element mesh is obtained using a Delaunay triangulation [49].
3. The alpha-shape method [22,84] is used to identify the external boundaries onto which the boundary conditions are imposed.
4. The nonlinear governing equations are solved for displacement, velocity and pressure at every node of the mesh.
5. Computed velocities and pressures are used to update the position of the particles.
6. Return to step 2 and repeat for the next time increment.

Thus, the PFEM can be interpreted as an updated Lagrangian approach, where the FEM is used to solve the incremental problem. In the PFEM, the mesh works as the background mesh for integration of the differential equations, and simultaneously, the mesh is used to keep track of free surfaces and contacts. Similar to the standard FEM, the accuracy of the solution in the PFEM depends on the mesh density and quality.

In a Lagrangian description of motion, the particles in the finite element mesh also represent material particles. Thus, the particles will move with the flow of the material. The motion of the particles might result in regions of increased concentration of particles and consequently regions where the particle spacing is large. The accuracy of the solution is affected if the distribution of particles becomes too irregular. In the present implementation of the PFEM, this issue is addressed by allowing the removal and addition of particles. A geometric criterion based on a characteristic element size and distance between particles governs the addition and removal of particles. In the PFEM, contact between the deforming material domain and fixed boundaries is detected automatically during the mesh generation, and no contact search algorithm is required. Penetration of the nodes of the deforming material into the fixed boundaries is prevented by the incompressibility condition. In the present implementation of the PFEM, frictional contact between the deforming domain and the fixed boundaries is modelled via the frictional resistance of the deforming material. More details regarding the automatic contact treatment of the PFEM can be found in [61].

3.4 Simulation procedures

The column collapse experiment was simulated using a two-dimensional plane deformation implementation of the PFEM. The granular material mass was represented using particles which were initially arranged in a regular rectangular pattern. The bottom surface and the left wall were modelled as stationary particles. The initial particle disposition and the location of the fixed particles used as boundaries are conceptually illustrated in Fig. 6. Throughout the present study, a stabilized linear triangular mixed velocity–pressure finite element formulation was used to solve the Lagrangian equations [18]. A fully implicit scheme was used for the time integration where the time step size was a function of the maximum velocity and the minimum distance between the particles. A maximum allowed value of the time step was set to $\Delta t = 1.0 \times 10^{-4}$ s, and a convergence criterion of 10^{-4} was used.

In the literature [44,52], the time evolution of the flow front in the column collapse is commonly described using a characteristic time scale based on the free-fall time of the granular column $\tau_c = \sqrt{h_i/g}$. In the present study, the simulations were terminated at the normalized time $\bar{t} = t/\tau_c = 4.0$, at which the flow front propagation was assumed to have ceased for the investigated range of aspect ratios. In a comprehensive experimental study of the collapse of granular columns along a horizontal channel, Lube et al. [52] derived a $\bar{t} = 3.3$. Thus, the assumption of a ceased flow front at $\bar{t} = 4.0$ is considered adequate and conservative. Since the granular materials in the present study were assumed to be dry and cohesionless, the
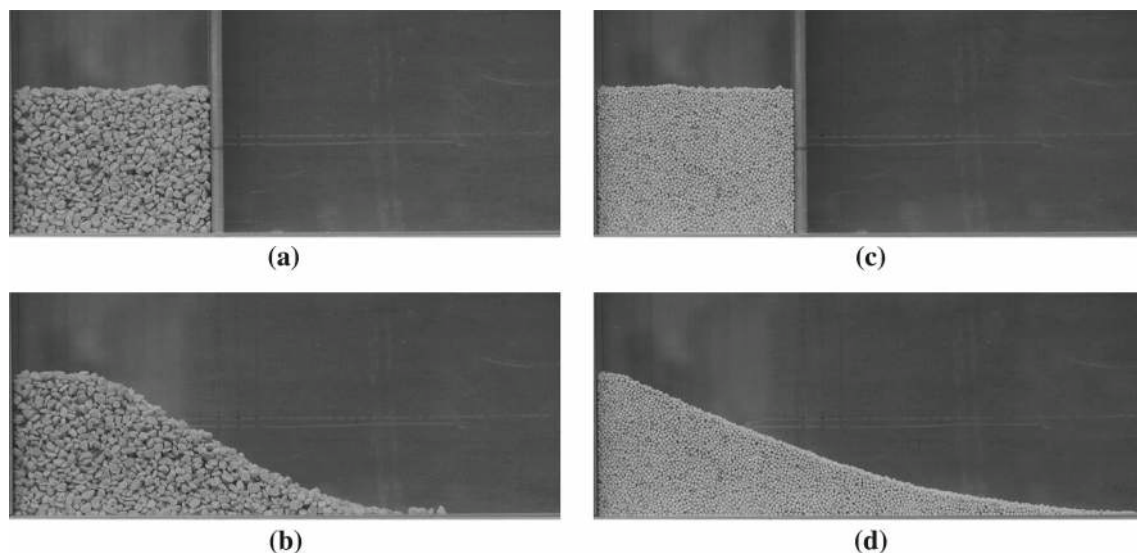
Fig. 7 Photographs of the initial configuration and final deposit of the rectangular channel column collapse experiments with low aspect ratios. (**a**) and (**b**) Test no. 1 for the KCl with $a_i = 0.73$ and $l_i = 100$ mm. (**c**) and (**d**) Test no. 1 for the Al_2O_3 with $a_i = 0.75$ and $l_i = 99$ mm
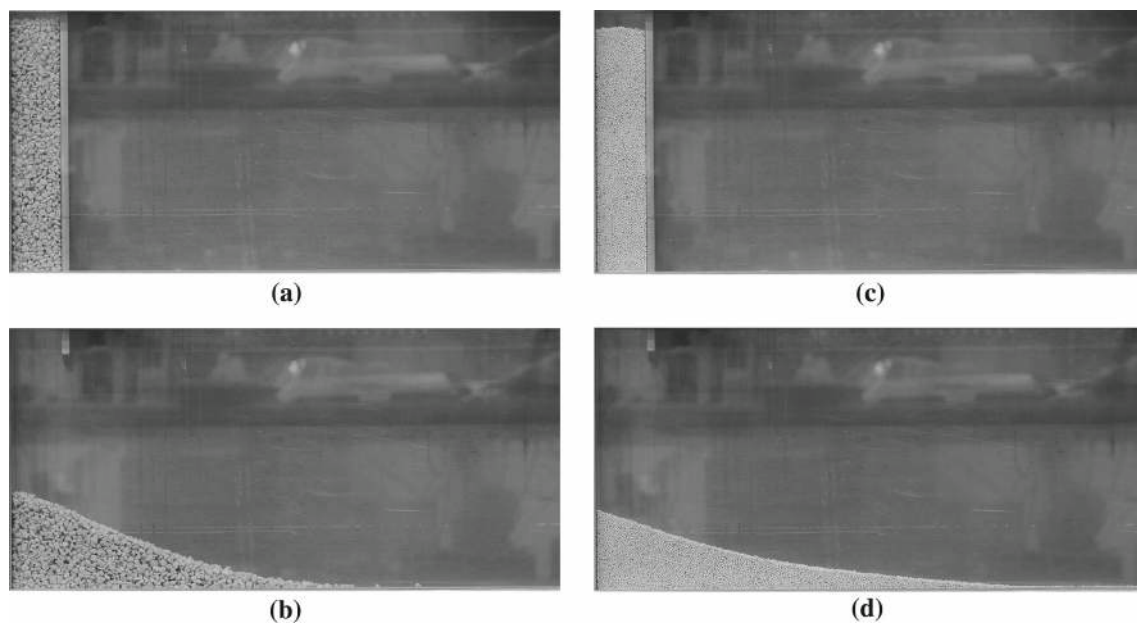

Fig. 8 Photographs of the initial configuration and final deposit of the rectangular channel column collapse experiments with high aspect ratios. (**a**) and (**b**) Test no. 3 for the KCl with $a_i = 5.13$ and $l_i = 39$ mm. (**c**) and (**d**) Test no. 3 for the Al_2O_3 with $a_i = 4.92$ and $l_i = 39$ mm

constitutive model parameter b_2, described in Sect. 3.2, was kept at a very small positive value ($b_2 = 10^{-6}$ Pa) in all the simulations. Since the granular materials were considered as incompressible, the choice of bulk modulus is arbitrary. The value of the bulk modulus was set to $\kappa = 2.2$ GPa, which corresponds to the bulk modulus of water. The computational time for the column collapse simulations on a 2.60 GHz Intel Xeon processor was between 5 and 160 minutes, depending on the size of the computational domain.

4 Results and discussion

In the following section, the experimental and numerical results are presented and discussed. The flow dynamics of the rectangular column collapse was investigated for a range of initial aspect ratios. The PFEM was used with two different constitutive models to simulate the experiments, using a two-dimensional plane deformation formulation. The numerical mesh convergence was studied, and the constitutive models were calibrated by inverse modelling. The constitutive
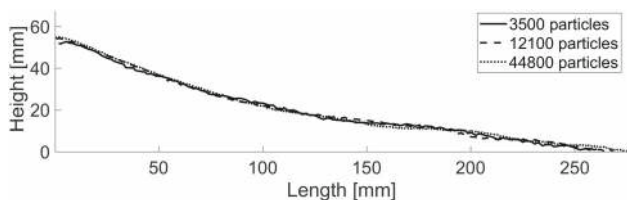
Fig. 9 Mesh size dependency of the final deposit profile extracted from the simulated rectangular column collapse with $a_i = 10$ and $l_i = 24\,\mathrm{mm}$
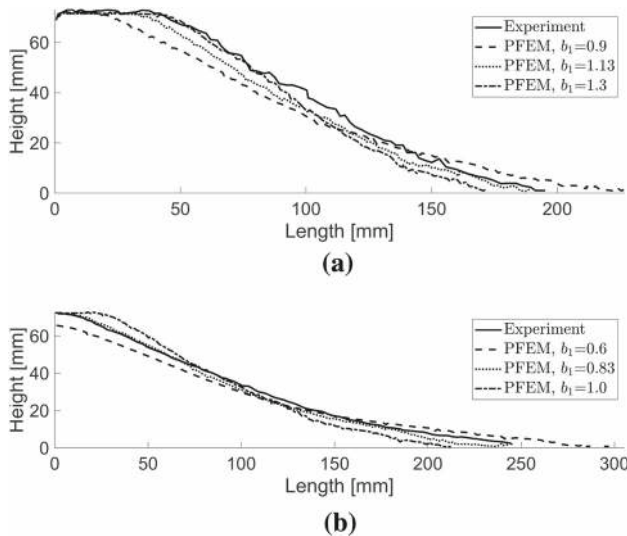

Fig. 10 Comparison of experimental and simulated final deposit profiles from the rectangular column collapse, for the calibration of the constitutive parameter b_1. (**a**) Test no. 3 for the KCl with $a_i = 0.73$ and (**b**) test no. 3 for the Al$_2$O$_3$ with $a_i = 0.75$

models were then evaluated and validated by comparing the numerical and experimental results for column collapses over a wide range of initial aspect ratios.

4.1 Experimental observations

The flow dynamics of the granular column collapse was studied experimentally for the two granular materials. A series of representative examples showing how the flow dynamics varied with the aspect ratio a_i are shown in Figs. 7 and 8. When the value of a_i was low (Fig. 7), the flow was contained in the top surface layer, and most of the granular mass was stationary during the collapse. The final deposit profile at low values of a_i had a characteristic truncated cone shape, where a large part of the granular mass remained undisturbed during the collapse. Increasing the value of a_i resulted in a larger proportion of the granular mass being disturbed during the collapse, and the final deposit profile converged to become increasingly more cone shaped.

It is noted from Figs. 7 and 8 that the two granular materials resulted in final deposit profiles of different shapes, for similar values of a_i. The KCl resulted in a lower value of l_∞ compared to that of the Al$_2$O$_3$, for both the low and the high a_i. Both granular materials resulted in similar values of h_∞ for the low a_i experiment, while h_∞ was larger for the KCl than that of the Al$_2$O$_3$ for high a_i. Thus, the properties of the granular materials had an effect on the flow dynamics and on the shape of the deposit profiles. The angular shape of the grains of the KCl yields a higher internal friction compared to the spherical grains of the Al$_2$O$_3$. Thus, the Al$_2$O$_3$ flows more easily than the KCl. These observations are in line with the results of previous studies [4,43], where it was
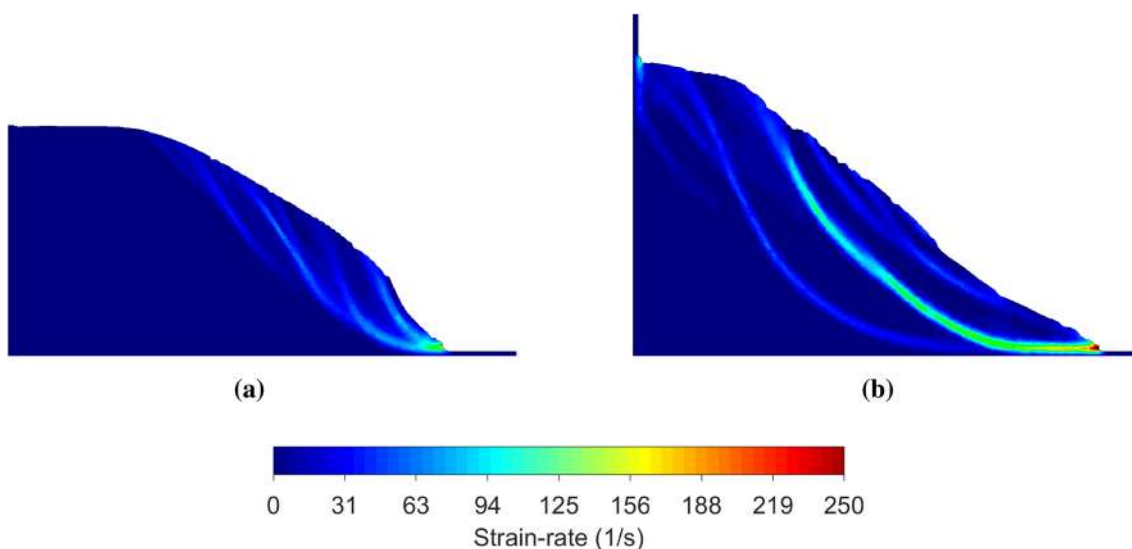
Fig. 11 Snapshots showing simulated strain rates during the column collapse for the KCl. (**a**) Test no. 1 with $a_i = 0.73$ and $l_i = 100$ mm and (**b**) test no. 3 with $a_i = 5.13$ and $l_i = 39$ mm. (**a**) and (**b**) The strain rate at the normalized time $\bar{t} = 1.4$ and with the constitutive parameter $b_1 = 1.13$
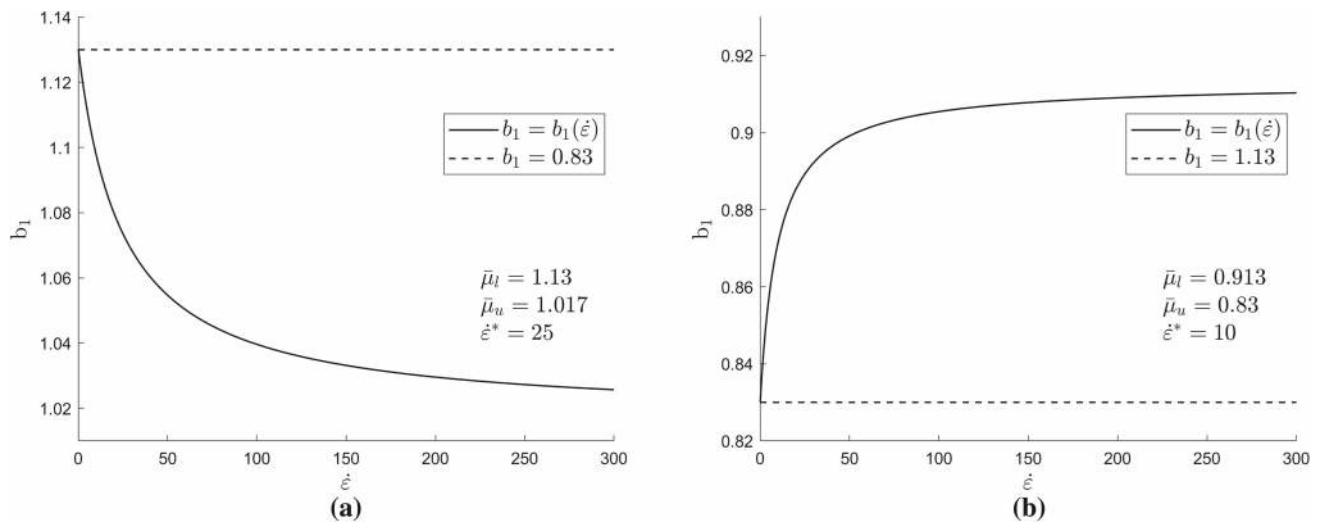
Fig. 12 Evolution of the constitutive model parameter b_1 as a function of strain rate $\dot{\varepsilon}$, obtained from calibration against experimental results for the column collapse. (**a**) The KCl and (**b**) the Al_2O_3

reported that the flow and spreading dynamics were mainly dependent on the value of a_i, but also on the internal friction of the granular materials.

It was observed that repeated experiments with the same input parameters resulted in slightly different final heights and lengths. This was expected, at least to some extent, since the nature of the granular material is very random and it is difficult to obtain exactly the same material distribution in the reservoir before each experiment. This observed randomness in the experiments is probably dominating over possible instrumentation errors.

4.2 Mesh convergence study

The mesh convergence of the current implementation of the PFEM was studied by running a test problem and varying the initial distance between the particles. For this, the rectangular granular column collapse problem with an initial height $h_i = 240$ mm and initial length $l_i = 24$ mm was chosen. The selected dimensions corresponded to $a_i = 10$. A high aspect ratio was selected to produce a case with large deformations and large pressure and velocity gradients. Three initial particle distances were selected: 1.5 mm, 0.75 mm and 0.375 mm, resulting in models containing approximately 3500, 12100 and 44800 particles, respectively. For the mesh convergence study, the flow formulation constitutive model was used with $b_1 = 1.0$ and $b_2 = 10^{-6}$ Pa. The bulk density was set to 1.00 g/cm^3. To evaluate the mesh size dependency, the final deposit profile was extracted and compared for the three models. In Fig. 9, the final deposit profiles are compared, showing that they are barely distinguishable. Thus, an initial particle distance of 1.5 mm was considered adequate and was used throughout the present study.
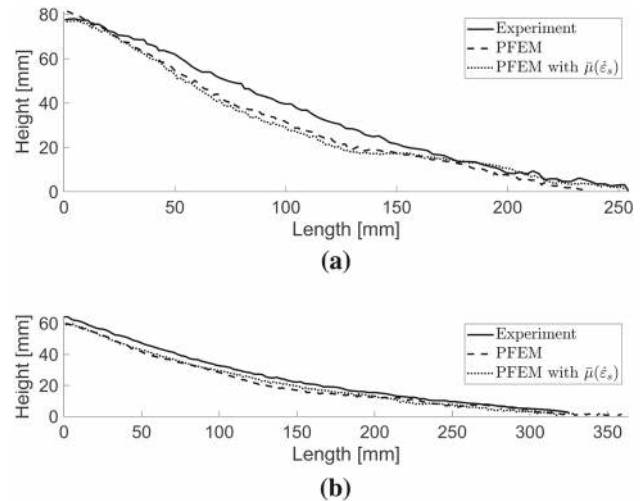
Fig. 13 Comparison of experimental and simulated final deposit profiles of the granular mass, for high aspect ratios. (**a**) Test no. 3 for the KCl with $a_i = 5.13$ and $l_i = 39$ mm and (**b**) test no. 3 for the Al_2O_3 with $a_i = 4.92$ and $l_i = 39$ mm

4.3 Constitutive model parameter calibration

The calibration of the constitutive model parameters was conducted in two steps, using the rectangular column collapse experiments. In the first step, the parameter b_1 was calibrated using a low aspect ratio experiment, with $a_i = 0.73$ for the KCl and $a_i = 0.75$ for the Al_2O_3. Experimental and simulated final deposit profiles were compared for different values of b_1, as shown in Fig. 10. In addition to comparing the shape of the deposit profile, the experimentally and numerically obtained values of h_∞ and l_∞ were also compared. From Fig. 10, it is observed that lowering the value of b_1 resulted in a less viscous behaviour of the granular mass, which is

Table 2 Experimental and simulated final length l_∞ and height h_∞ from the series of column collapse experiments for KCl. Tests 1–3 were used for calibration and tests 4–17 for validation

| Test	a_i	Experiment		PFEM				PFEM with $\bar{\mu}(\dot{\varepsilon}_s)$			
		l_∞ [mm]	h_∞ [mm]	l_∞ [mm]	$\%_{error}$	h_∞ [mm]	$\%_{error}$	l_∞ [mm]	$\%_{error}$	h_∞ [mm]	$\%_{error}$
1	0.73	196	72	195	0.5	72	0	198	1.0	72	0
2	2.15	228	80	219	3.9	84	5.0	225	1.3	83	3.8
3	5.13	254	77	236	7.1	81	5.2	256	0.8	77	0
4	5.23	193	60	185	4.1	60	0	60	8.8	210	10.0
5	1.58	177	72	181	2.3	74	2.8	192	8.5	67	6.9
6	9.60	85	22	83	2.4	23	4.5	96	12.9	22	0
7	0.83	204	81	202	1.0	81	0	218	6.9	81	0
8	3.04	222	78	235	5.9	80	2.6	251	13.1	72	7.7
9	3.07	150	44	130	13.3	46	4.5	146	2.7	43	2.3
10	2.08	190	65	181	4.7	66	1.5	199	4.7	62	4.6
11	6.20	147	40	136	7.5	42	5.0	149	1.4	39	2.5
12	6.30	75	19	69	8.0	20	5.3	73	2.7	19	0
13	7.90	154	46	163	5.8	45	2.2	178	15.6	41	10.9
14	8.45	171	49	164	4.1	47	4.1	182	6.4	43	12.2
15	1.02	142	54	136	4.2	59	9.3	143	0.7	57	5.6
16	1.19	225	97	227	0.9	100	3.1	247	9.8	92	5.2
17	4.05	240	69	216	10.0	74	7.2	235	2.1	65	5.8
Median $\%_{error}^a$					4.5		3.6		6.6		5.4

[a]Calculated from tests 4–17

Table 3 Experimental and simulated final length l_∞ and height h_∞ from the series of column collapse experiments for Al$_2$O$_3$. Tests 1–3 were used for calibration and tests 4–17 for validation

Test	a_i	Experiment		PFEM				PFEM with $\bar{\mu}(\dot{\varepsilon}_s)$			
		l_∞ [mm]	h_∞ [mm]	l_∞ [mm]	$\%_{error}$	h_∞ [mm]	$\%_{error}$	l_∞ [mm]	$\%_{error}$	h_∞ [mm]	$\%_{error}$
1	0.73	243	72	245	0.8	72	0	236	2.9	72	0
2	2.15	290	67	307	5.9	66	1.5	290	0	66	1.5
3	5.13	327	63	353	8.0	60	4.8	324	0.9	60	4.8
4	5.23	220	44	247	12.3	43	2.3	236	7.3	44	0
5	1.58	214	55	218	1.9	56	1.8	211	1.4	57	3.6
6	9.60	313	87	345	10.2	85	2.3	315	0.6	87	0
7	0.83	120	17	125	4.2	18	5.9	122	1.7	19	11.8
8	3.04	240	64	240	0	65	1.6	224	6.7	65	1.6
9	3.07	215	47	213	0.9	46	2.1	206	4.2	47	0
10	2.08	100	22	106	6.0	23	4.5	89	11.0	23	4.5
11	6.20	193	38	202	4.7	38	0	187	3.1	39	2.6
12	6.30	183	32	195	6.6	31	3.1	184	0.5	33	3.1
13	7.90	87	16	88	1.1	15	6.3	92	5.7	16	0
14	8.45	223	35	239	7.2	33	5.7	215	3.6	34	2.9
15	1.02	225	37	240	6.7	34	8.1	224	0.4	36	2.7
16	1.19	96	17	115	19.8	17	0	110	14.6	18	5.9
17	4.05	201	57	208	3.5	59	4.4	192	4.5	59	4.4
Median $\%_{error}^a$					5.3		2.7		3.9		2.8

[a]Calculated from tests 4–17

Fig. 14 Comparison of experimental and simulated normalized final height h_∞ as a function of the initial aspect ratio a_i from the rectangular column collapse. (**a**) The KCl and (**b**) the Al_2O_3


(a)

(b)
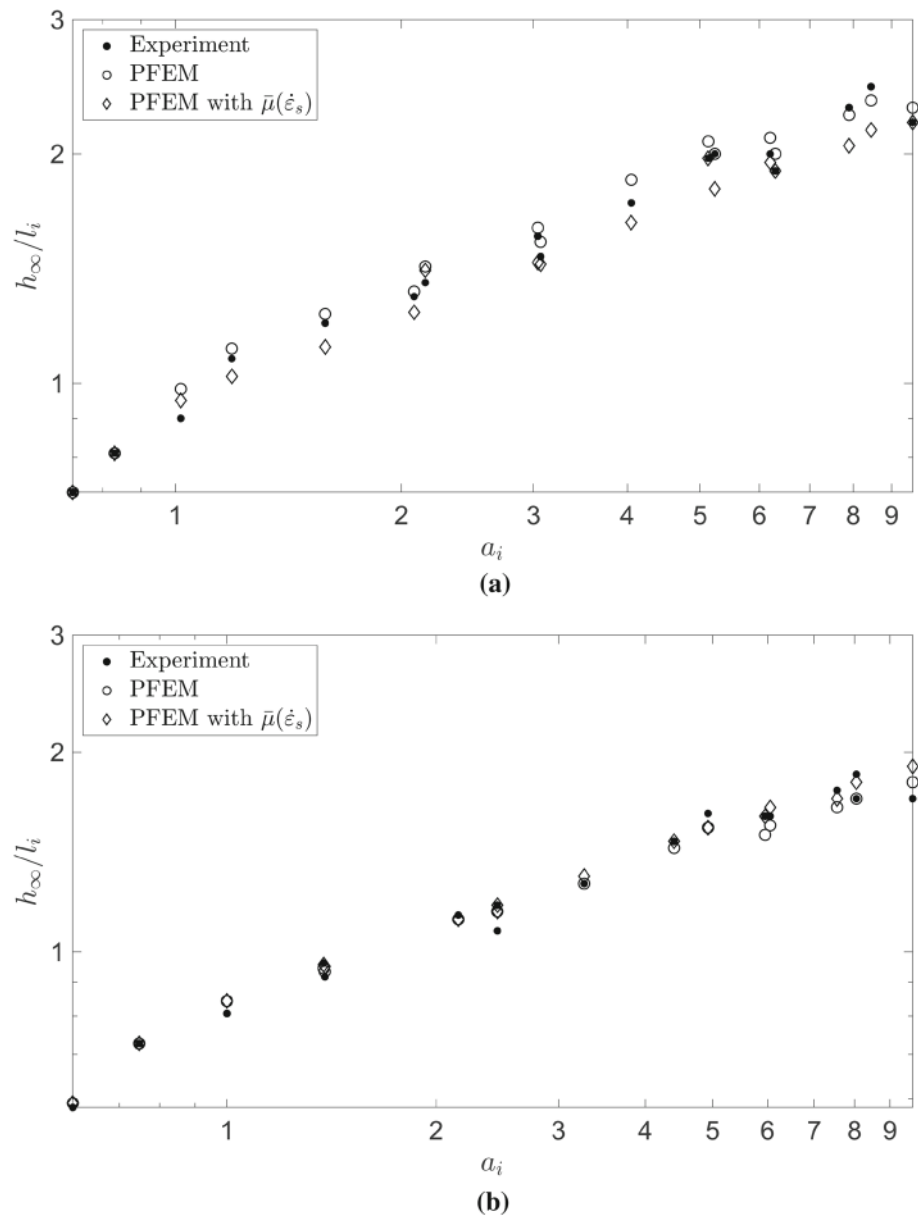
reflected in a larger simulated value of l_∞ for both materials. Increasing the value of b_1 resulted in a more viscous behaviour and thus a smaller simulated value of l_∞ for both materials and an increased value of h_∞ for the Al_2O_3, for the range of investigated values of b_1. Thus, b_1 was adjusted to obtain a good fit to the experimental values of h_∞ and l_∞. The value of b_1 that resulted in the most accurate prediction of the experimentally obtained h_∞ and l_∞ was obtained for the KCl ($b_1 = 1.13$) and for the Al_2O_3 ($b_1 = 0.83$).

The flow formulation constitutive model was then used with the obtained values of b_1 to simulate two additional experiments with increasingly larger aspect ratios. Experiments where $a_i = 2.15$ and $a_i = 5.13$ for the KCl and $a_i = 2.15$ and $a_i = 4.92$ for the Al_2O_3 were considered.

Increasing the value of a_i resulted in increasing strain rates during the column collapse, as shown in Fig. 11. The value of b_1 obtained through the initial calibration failed to predict h_∞ and l_∞ for the experiments with larger a_i, for both the KCl and for the Al_2O_3. For the KCl, h_∞ was overpredicted, while l_∞ was underpredicted for increasing values of a_i, indicating that a $b_1 = 1.13$ overpredicted the material strength at increasing strain rates. For the Al_2O_3, it was the other way around, h_∞ was underpredicted, while l_∞ was overpredicted for increasing values of a_i, indicating that a $b_1 = 0.83$ underpredicted the material strength at increasing strain rates.

Thus, to accurately model the rectangular column collapse at increasing values of a_i required a constitutive model able

Fig. 15 Comparison of experimental and simulated normalized final length l_∞ as a function of the initial aspect ratio a_i from the rectangular column collapse. (**a**) The KCl and (**b**) the Al_2O_3
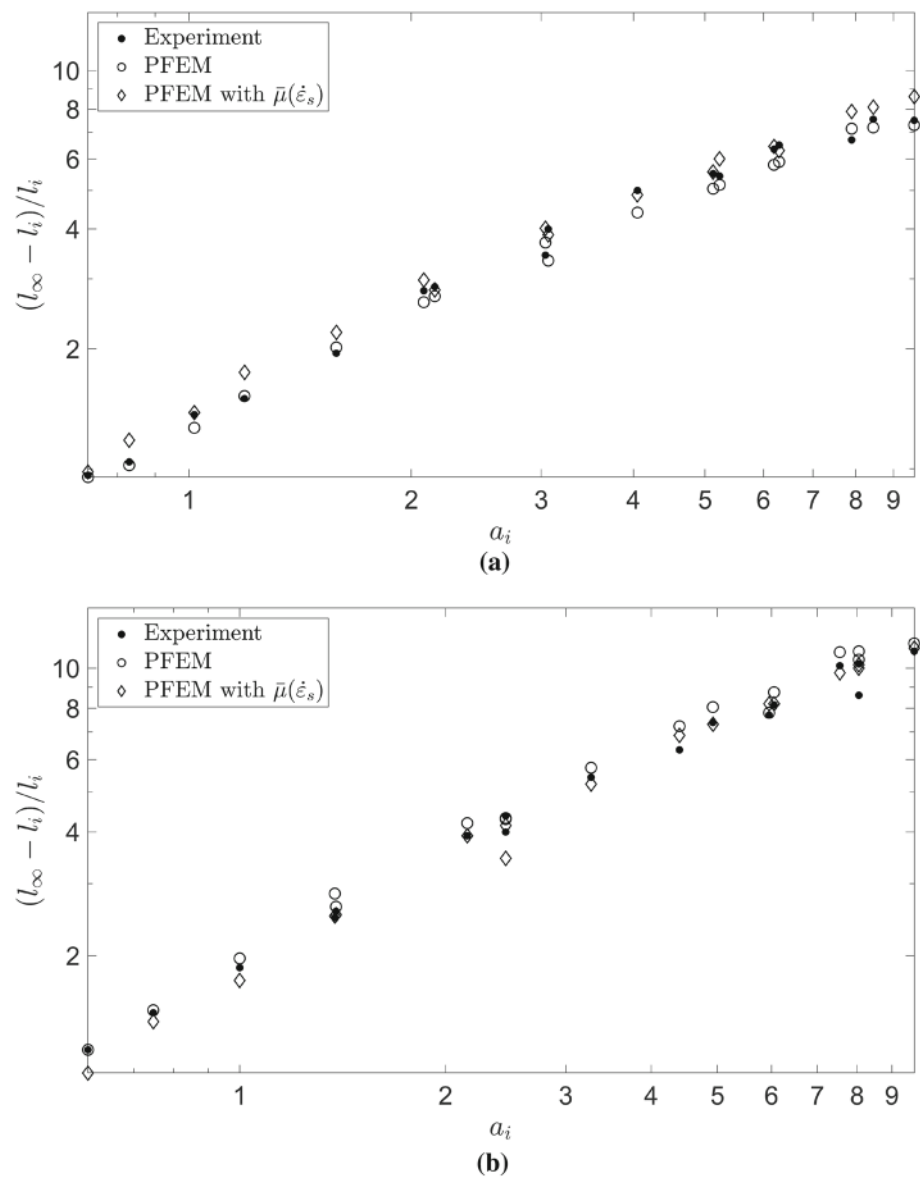

to account for the strain-rate-dependent material strength. The second constitutive model of the present study allows the internal coefficient of friction (the parameter b_1) of the material to be dependent on the strain rate. This model requires the definition of some additional parameters governing the evolution of the residual resistance $\bar{\mu}$, which is equal to b_1 for a granular material in which the effect of dilatancy can be neglected. As presented in Sect. 3.2.2, these parameters are the lower and upper bounds of $\bar{\mu}$ ($\bar{\mu}_l$ and $\bar{\mu}_u$) and the equivalent deviatoric shear strain rate $\dot{\varepsilon}_s^*$.

In the literature [3,40,50], the identification of model parameters corresponding to $\bar{\mu}_l$ and $\bar{\mu}_u$ has been discussed. The proposed relationships between the quasi-static material strength and the material strength at high strain rates vary depending on the granular material and the type of flow considered. It is thus difficult to know this relationship a priori

for arbitrary granular materials and flow conditions. In the present study, the choice of relationship between $\bar{\mu}_l$ and $\bar{\mu}_u$ was based on experimental observations from the column collapses. For the KCl, the value of $\bar{\mu}_l$ was set to be equal to the previously obtained value of $b_1 = 1.13$, while the value of $\bar{\mu}_u$ was set to $0.9 \times b_1$. Thus, the residual resistance was set to decrease with increasing strain rate. For the Al_2O_3, the value of $\bar{\mu}_l$ was set equal to $b_1 = 0.83$ and the value of $\bar{\mu}_u$ was set to $1.1 \times b_1$. Thus, $\bar{\mu}$ was set to increase with increasing strain rate.

The remaining model parameter $\dot{\varepsilon}_s^*$ governs the transition between $\bar{\mu}_l$ and $\bar{\mu}_u$ with increasing strain rate shown conceptually in Fig. 5. The value of $\dot{\varepsilon}_s^*$ was obtained using three column collapse experiments, where a_i was varied between 0.73 and 5.13 for the KCl and between 0.75 and 4.92 for the Al_2O_3. The same procedure that was used to calibrate b_1 was
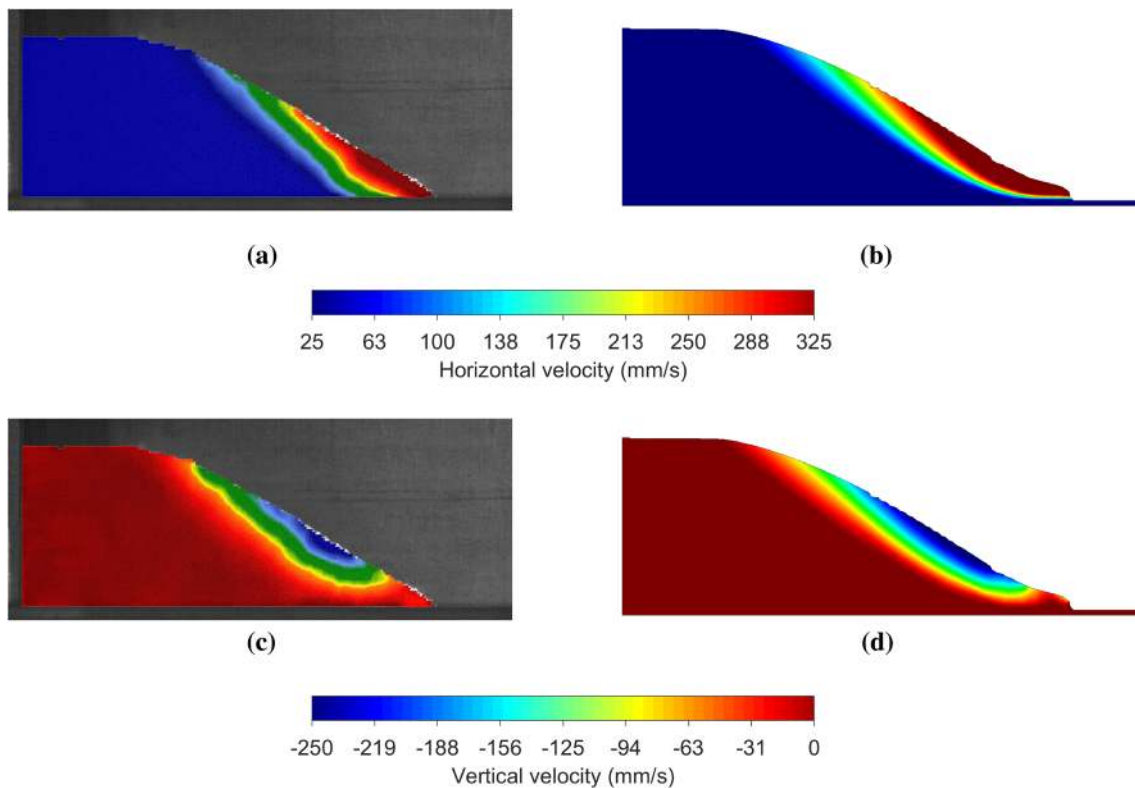
Fig. 16 Comparison of the in-plane velocity fields during the column collapse for the Al_2O_3. Measured using DIC (left column) and simulated using the PFEM with the strain-rate-dependent residual strength constitutive model (right column). The horizontal component of the velocity is compared in (**a**)–(**b**), and the vertical component is compared in (**c**)–(**d**). Results are from test no. 18 with $a_i = 0.60$ and $l_i = 80$ mm. The results are compared at the normalized time $\bar{t} = 1.8$

employed to calibrate $\dot{\varepsilon}_s^*$. The shape of the final deposit and the values of h_∞ and l_∞ were compared for different values of $\dot{\varepsilon}_s^*$. The best match to the experimentally obtained h_∞ and l_∞ was obtained with $\dot{\varepsilon}_s^* = 25$ for the KCl and $\dot{\varepsilon}_s^* = 10$ for the Al_2O_3. In Fig. 13, the shape of the deposits obtained experimentally and with the two constitutive models of the present work is shown for the KCl and the Al_2O_3. The evolution of the parameter b_1 as a function of the strain rate is shown in Fig. 12 for both granular materials.

The discrepancy between the experimental and the simulated deposit profiles in Fig. 13 is slight for the Al_2O_3, but more prominent for the KCl. A possible explanation is that the assumption of using a continuum representation of a discrete media might be questionable in the case of KCl. To accurately model a discrete media as a continuum requires that the particles are much smaller than the smallest characteristic dimension of the process considered [21]. The size and the angular shape of the grains of the KCl, and the length scale of the experiments of the present study cause the flowing layer of grains to be thin in comparison with the grain size in some of the experiments, thus making the continuum representation questionable at that location. A further possible explanation for the discrepancy is that the shape of the

grains of the KCl might result in some dilatation during the column collapse, thus resulting in a slight volume increase. The dilatation is typically small for a granular material in the fluid-like state [25], and it is typically neglected. In the present study, the granular materials are modelled as incompressible; thus, any dilatation is not taken into account which is an additional contributing factor to the slight deviation between simulated and experimental profiles for the KCl.

It must also be noted that when using the PFEM, the remeshing method may cause a slight variation of the volume of the computational domain. To prevent this, the choice of the value of the alpha-shape parameter should be carefully considered. The issue of volume conservation and remeshing in the PFEM is discussed in detail in [26] where it is suggested that values of the alpha-shape parameter close to 1.2 keep the volume variation at acceptable levels for problems of highly unsteady flows. Thus, throughout the present study, the value of the alpha-shape parameter was set to 1.2.

In the present study, a strategy for calibration of the constitutive parameters based on a comparison between experimental and simulated column collapses is presented. Using this approach, a set of constitutive parameters were obtained for the two granular materials. To obtain a unique
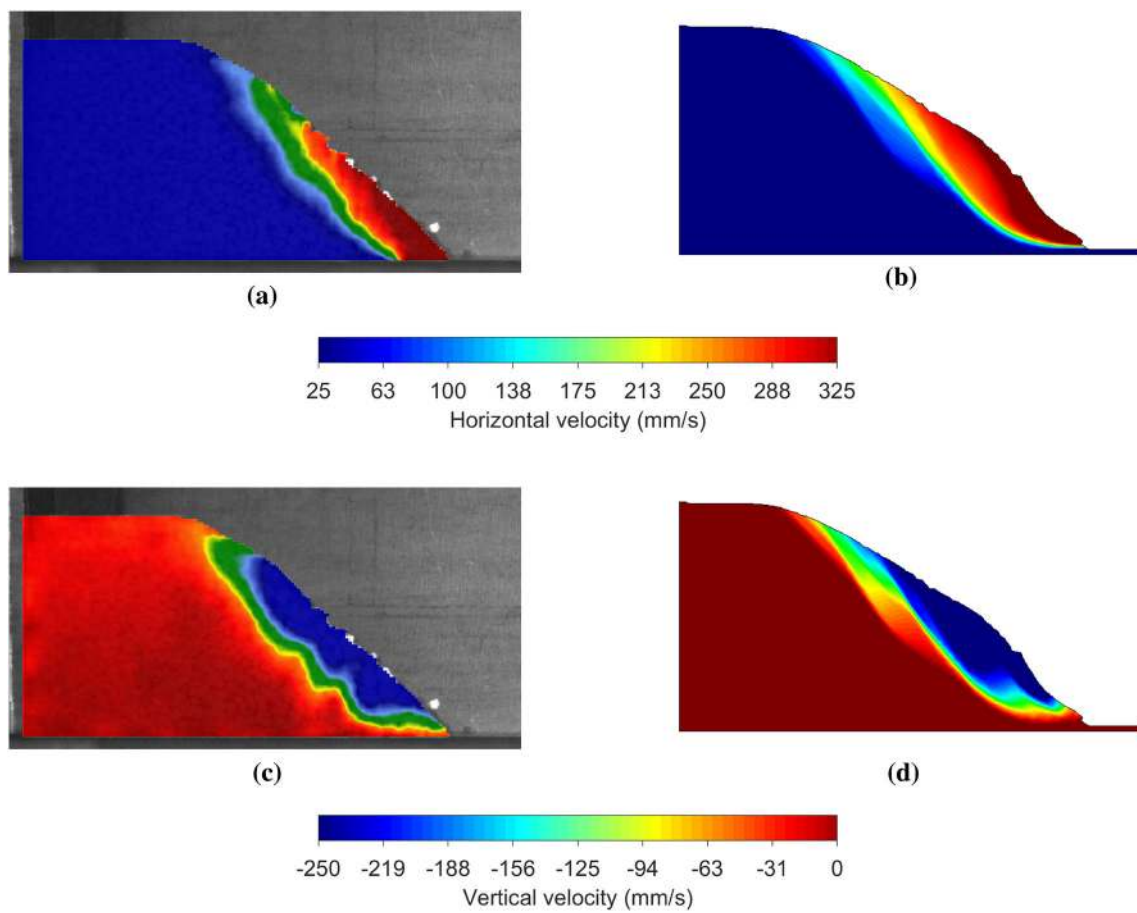
Fig. 17 Comparison of the in-plane velocity fields during the column collapse for the KCl. Measured using DIC (left column) and simulated using the PFEM with the strain-rate-dependent residual strength constitutive model (right column). The horizontal component of the velocity is compared in (**a**)–(**b**), and the vertical component of it is compared in (**c**)–(**d**). Results are from test no. 18 with $a_i = 0.83$ and $l_i = 72$ mm. The results are compared at the normalized time $\bar{t} = 1.4$

set of constitutive parameters is indeed a difficult task, partly because it is difficult to experimentally measure the evolution of the frictional resistance as a function of the strain rate in a granular material. Thus, the parameters obtained in this study are considered to be of use in the present application and at the investigated loading conditions. A strategy to obtain a unique set of constitutive parameters for arbitrary loading conditions and granular materials would indeed be an improvement but lies outside the scope of the present study.

4.4 Model validation

To validate the proposed numerical model, a number of column collapses with varying a_i were simulated and compared to experimental results. In total, the 17 cases from Table 1 were simulated for each granular material, where a_i was varied between 0.73 and 9.60 for the KCl and between 0.60 and 9.70 for the Al_2O_3. Experimental and simulated values of l_∞ and $h_\infty$ are presented in Tables 2 and 3. The experimentally measured h_∞ and l_∞ were normalized with respect to the initial length l_i and were plotted as a function of a_i, using a logarithmic scale on both the horizontal and the vertical axes, as shown in Figs. 14 and 15. The normalized h_∞ and l_∞ obtained from the simulations were plotted together with the experimental results, as shown in Figs. 14 and 15. When comparing the experimental and numerical h_∞ and l_∞, it is observed that the strain-rate-dependent residual strength constitutive model is able to accurately predict the column collapse at the investigated range of a_i, for both the KCl and the Al_2O_3. An error percentage for simulated l_∞ and h_∞ compared to experimental results was calculated and the median of the error percentage was determined, excluding the tests used for calibration of $\dot{\varepsilon}_s^*$, as given in Tables 2 and 3. For the KCl, comparing the median percentage errors, the most accurate prediction was obtained for the constitutive model without strain-rate-dependent residual strength. For the Al_2O_3, the strain-rate-dependent residual strength model resulted in a more accurate prediction of l_∞, while for h_∞ a

similar accuracy was obtained for both constitutive models. The best model predictions resulted in median percentage errors less than 5, for both granular materials.

To further compare the experimentally observed flow dynamics to the PFEM simulations, the horizontal and vertical velocity fields were extracted from the column collapse experiment using DIC, as described in Sect. 2.2. In Figs. 16 and 17, the horizontal and vertical velocity fields are compared for the Al_2O_3 with $a_i = 0.60$ and $l_i = 80$ mm and for the KCl with $a_i = 0.83$ and $l_i = 72$ mm. Compared to the experimentally measured velocities, the proposed strain-rate-dependent residual strength model was able to predict the flow dynamics of the column collapse accurately. Furthermore, the time evolution of the column height during the collapse was measured experimentally from the high-speed recording of test no. 19, for both the KCl and the Al_2O_3. The test was simulated, and the time evolution is compared in Fig. 18. The PFEM model resulted in a slight underprediction of the time it takes for the column to settle, with a more accurate prediction for the Al_2O_3 compared to that of the KCl. A possible reason for the underprediction is that the vertical removal of the door is not included in the simulation. The finite time required to remove the door in the experiments might affect the flow dynamics, causing a lower vertical velocity of the top layer of the column during the collapse, compared to a collapse where the door is not included.

In the present implementation of the PFEM, friction between granular materials and surrounding structures is not treated explicitly. This is due to the use of the incompressibility condition to model the interaction between the deforming domain and the fixed boundaries. Thus, the granular material strength governs the flow at the interface between granular mass and fixed boundaries. The use of a simplified contact treatment is given some validity from an experimental study by Lube et al. [51], where column collapses of a number of different granular materials were conducted on three different surfaces: a smooth wooden surface, a smooth plastic surface and a rough surface made of sand paper. The authors found that the shape of the deposits was not significantly affected by the surface properties. It was suggested that a possible explanation for the independence of surface friction was the development of a dynamic interface a few particles from the base surface, separating the flow between stationary and moving granular material.

It should be noted that regardless of the choice of numerical model for the transient granular material flow, validation has to be performed to ensure reliable model predictions. The accurate DIC measurements of the granular material flow dynamics provided a foundation to assess the validity of the proposed PFEM model. In this work, a two-dimensional PFEM model was applied and validated for the fundamental problem of collapsing rectangular columns.
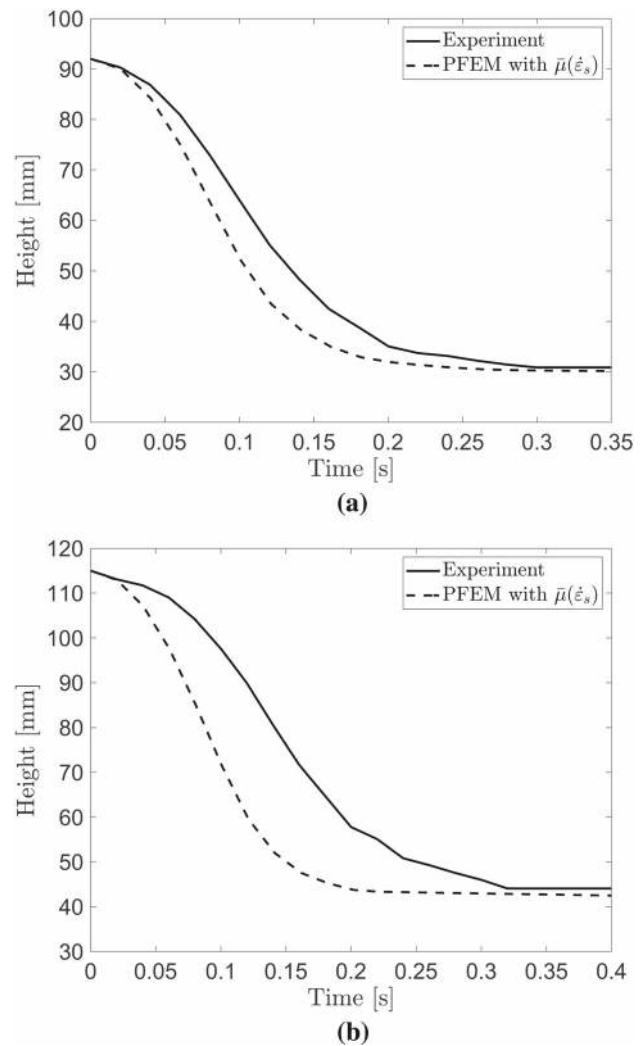
Fig. 18 Comparison of experimental and simulated time evolution of column height during the collapse. Results are from test no. 19, and the simulations were performed using the strain-rate-dependent residual strength constitutive model. (a) The Al_2O_3 with $a_i = 4.38$ and $l_i = 21$ mm and (b) the KCL with $a_i = 5.23$ and $l_i = 22$ mm

5 Conclusions

The particle finite element method (PFEM) is used to model the transient granular material flow of a collapsing rectangular column. A novel experimental methodology for quantification of the flow dynamics of the collapsing column of granular material is designed. The experimental results are used to calibrate and validate the proposed numerical model. A conclusion from the present study is that the flow dynamics of the column collapse can be quantified by measuring the in-plane velocity field using digital image correlation. A numerical model, where the PFEM is used with two strain-rate-dependent constitutive models, is evaluated and compared to experimental results. It is concluded that the PFEM model of the present study accurately predicts the

flow dynamics of the column collapse for two granular materials with different material properties and over a range of aspect ratios. By validation, it is shown that the strain-rate-dependent residual strength constitutive model is the most accurate for the Al_2O_3. In general, the best model prediction is obtained for the Al_2O_3, while some discrepancy between experimental and simulated results is observed for the KCl. One possible cause of the discrepancy is that the length scale of the granular material flow is too small for the KCl to accurately model it as a continuum. The proposed novel strain-rate-dependent residual strength constitutive model requires the calibration of only three parameters, the lower and upper bounds of the residual resistance $\bar{\mu}_l$ and $\bar{\mu}_u$ and the equivalent deviatoric shear strain rate parameter $\dot{\varepsilon}_s^*$. The number of parameters of the proposed model is low compared to other numerical methods commonly used for the simulation of granular material flow, such as the DEM. In conclusion, the proposed PFEM model is a robust numerical tool that is useful for modelling transient granular material flow.

Compliance with ethical standards

References

1. Andersen S, Andersen L (2010) Modelling of landslides with the material-point method. Comput Geosci 14(1):137–147
2. Andrade JE, Ellison KC (2008) Evaluation of a predictive constitutive model for sands. J Geotech Geoenviron Eng 134(12):1825–1828
3. Andrade JE, Chen Q, Le PH, Avila CF, Matthew Evans T (2012) On the rheology of dilative granular media: bridging solid- and fluid-like behavior. J Mech Phys Solids 60(6):1122–1136
4. Balmforth NJ, Kerswell RR (2005) Granular collapse in two dimensions. J Fluid Mech 538:399–428
5. Bui HH, Fukagawa R, Sako K, Ohno S (2008) Lagrangian meshfree particles method (SPH) for large deformation and failure flows of geomaterial using elastic-plastic soil constitutive model. Int J Numer Anal Methods Geomech 32(12):1537–1570
6. Bui HH, Fukagawa R, Sako K, Wells JC (2011) Slope stability analysis and discontinuous slope failure simulation by elasto-plastic smoothed particle hydrodynamics (SPH). Géotechnique 61:565–574
7. Cabiscol R, Finke JH, Kwade A (2018) Calibration and interpretation of DEM parameters for simulations of cylindrical tablets with multi-sphere approach. Powder Technol 327:232–245
8. Cante JC, Riera MD, Oliver J, Prado JM, Isturiz A, Gonzalez C (2011) Flow regime analyses during the filling stage in powder metallurgy processes: experimental study and numerical modelling. Granul Matter 13(1):79–92
9. Cante JC, Dávalos C, Hernández JA, Oliver J, Jonsén P, Gustafsson G, Häggblad H (2014) PFEM-based modeling of industrial granular flows. Comput Part Mech 1(1):47–70
10. Chen Z, Hu W, Shen L, Xin X, Brannon R (2002) An evaluation of the MPM for simulating dynamic failure with damage diffusion. Eng Fract Mech 69(17):1873–1890
11. Cremonesi M, Frangi A, Perego U (2011) A Lagrangian finite element approach for the simulation of water-waves induced by landslides. Comput Struct 89(11–12):1086–1093
12. Cremonesi M, Ferri F, Perego U (2017) A basal slip model for Lagrangian finite element simulations of 3D landslides. Int J Numer Anal Methods Geomech 41(1):30–53
13. Crosta GB, Imposimato S, Roddeman D (2009) Numerical modeling of 2-D granular step collapse on erodible and nonerodible surface. J Geophys Res Solid Earth 114(3):1–19
14. Crosta GB, Imposimato S, Roddeman D (2015) Granular flows on erodible and non erodible inclines. Granul Matter 17(5):667–685
15. Cundall PA, Strack ODL (1979) A discrete numerical model for granular assemblies. Géotechnique 29(1):47–65
16. Dávalos C, Cante J, Hernández JA, Oliver J (2015) On the numerical modeling of granular material flows via the particle finite element method (PFEM). Int J Solids Struct 71:99–125
17. Desai CS, Siriwardane HJ (1984) Constitutive laws for engineering materials, with emphasis on geologic materials. Prentice-Hall, Englewood Cliffs
18. Dohrmann CR, Bochev PB (2004) A stabilized finite element method for the Stokes problem based on polynomial pressure projections. Int J Numer Methods Fluids 46(2):183–201
19. Drucker D, Prager W (1952) Soil mechanics and plastic analysis or limit design. Q Appl Math 9(2):157–165
20. Dunatunga S, Kamrin K (2015) Continuum modelling and simulation of granular flows through their many phases. J Fluid Mech 779:483–513
21. Duran J (2000) Sands, powders, and grains : an introduction to the physics of granular materials. Springer, New York
22. Edelsbrunner H, Mücke EP (1994) Three-dimensional alpha shapes. ACM Trans Graph 13(1):43–72
23. Elaskar SA, Godoy LA, Gray DD, Stiles JM (2000) A viscoplastic approach to model the flow of granular solids. Int J Solids Struct 37(15):2185–2214
24. Fern EJ, Soga K (2016) The role of constitutive models in MPM simulations of granular column collapses. Acta Geotech 11(3):659–678
25. Forterre Y, Pouliquen O (2008) Flows of dense granular media. Annu Rev Fluid Mech 40(1):1–24

26. Franci A, Cremonesi M (2017) On the effect of standard PFEM remeshing on volume conservation in free-surface fluid flow problems. Comput Part Mech 4(3):331–343

27. Gan JQ, Zhou ZY, Yu AB (2016) A GPU-based DEM approach for modelling of particulate systems. Powder Technol 301:1172–1182

28. Gingold RA, Monaghan JJ (1977) Smoothed particle hydrodynamics: theory and application to non-spherical stars. Mon Not R Astron Soc 181(3):375–389

29. GOM GmbH (2007) ARAMIS User Manual - Software v6.1. Braunschweig

30. Hurley RC, Andrade JE (2017) Continuum modeling of rate-dependent granular flows in SPH. Comput Part Mech 4(1):119–130

31. Iaconeta I, Larese A, Rossi R, Guo Z (2017) Comparison of a material point method and a galerkin meshfree method for the simulation of cohesive-frictional materials. Materials 10(10):1150

32. Iaconeta I, Larese A, Rossi R, Oñate E (2019) A stabilized mixed implicit material point method for non-linear incompressible solid mechanics. Comput Mech 63(6):1243–1260

33. Idelsohn SR, Oñate E, Del Pin F (2003) A Lagrangian meshless finite element method applied to fluid-structure interaction problems. Comput Struct 81(8–11):655–671

34. Idelsohn SR, Oñate E, Del Pin F (2004) The particle finite element method: a powerful tool to solve incompressible flows with free-surfaces and breaking waves. Int J Numer Methods Eng 61:964–989

35. Jaeger HM, Nagel SR, Behringer RP (1996) Granular solids, liquids, and gases. Rev Mod Phys 68(4):1259–1273

36. Jarray A, Magnanimo V, Luding S (2019) Wet granular flow control through liquid induced cohesion. Powder Technol 341:126–139

37. Jonsén P, Pålsson B, Häggblad H (2012) A novel method for full-body modelling of grinding charges in tumbling mills. Miner Eng 33:2–12

38. Jonsén P, Pålsson B, Stener J, Häggblad H (2014) A novel method for modelling of interactions between pulp, charge and mill structure in tumbling mills. Miner Eng 63:65–72

39. Jonsén P, Stener JF, Pålsson BI, Häggblad H (2015) Validation of a model for physical interactions between pulp, charge and mill structure in tumbling mills. Miner Eng 73:77–84

40. Jop P, Forterre Y, Pouliquen O (2006) A constitutive law for dense granular flows. Nature 441:727–730

41. Kajberg J, Lindkvist G (2004) Characterisation of materials subjected to large strains by inverse modelling based on in-plane displacement fields. Int J Solids Struct 41(13):3439–3459

42. Karlsson T, Klisinski M, Runesson K (1998) Finite element simulation of granular material flow in plane silos with complicated geometry. Powder Technol 99(1):29–39

43. Lajeunesse E, Mangeney-Castelnau A, Vilotte JP (2004) Spreading of a granular mass on a horizontal plane. Phys Fluids 16(7):2371–2381

44. Lajeunesse E, Monnier JB, Homsy GM (2005) Granular slumping on a horizontal surface. Phys Fluids 17(10):1–15

45. Larese A (2017) A Lagrangian PFEM approach for non-Newtonian viscoplastic materials. Rev Int Metodos Numer Calc Disen Ing 33(3–4):307–317

46. Larese A, Rossi R, Oñate E, Toledo M, Morán R, Campos H (2015) Numerical and experimental study of overtopping and failure of rockfill dams. Int J Geomech 15(4):1–23

47. Larsson S, Gustafsson G, Oudich A, Jonsén P, Häggblad HH (2016) Experimental methodology for study of granular material flow using digital speckle photography. Chem Eng Sci 155:524–536

48. Larsson S, Gustafsson G, Häggblad H, Jonsén P (2017) Experimental and numerical study of potassium chloride flow using smoothed particle hydrodynamics. Miner Eng 116:88–100

49. Lee DT, Schachter BJ (1980) Two algorithms for constructing a Delaunay triangulation. Int J Comput Inf Sci 9(3):219–242

50. Liang Df, He Xz (2014) A comparison of conventional and shear-rate dependent Mohr–Coulomb models for simulating landslides. J Mt Sci 11(6):1478–1490

51. Lube G, Huppert HE, Sparks RSJ, Hallworth MA (2004) Axisymmetric collapses of granular columns. J Fluid Mech 508:175–199

52. Lube G, Huppert HE, Stephen R, Sparks J, Freundt A (2005) Collapses of two-dimensional granular columns. Phys Rev E 72:041301

53. Lucy LB (1977) A numerical approach to the testing of the fission hypothesis. Astron J 82(12):1013–1024

54. Manzari MT, Dafalias YF (1997) A critical state two-surface plasticity model for sands. Géotechnique 47(2):255–272

55. Mast CM, Arduino P, Mackenzie-Helnwein P, Miller GR (2014) Simulating granular column collapse using the material point method. Acta Geotech 10(1):101–116

56. Midi G (2004) On dense granular flows. Eur Phys J E 14(4):341–365

57. Nguyen CT, Nguyen CT, Bui HH, Nguyen GD, Fukagawa R (2017) A new SPH-based approach to simulation of granular flows using viscous damping and stress regularisation. Landslides 14(1):69–81

58. Nonoyama H, Moriguchi S, Sawada K, Yashima A (2015) Slope stability analysis using smoothed particle hydrodynamics (SPH) method. Soils Found 55(2):458–470

59. Oliver J, Cante JC, Weyler R, González C, Hernandez J (2007) Particle finite element methods in solid mechanics problems. In: Oñate E, Owen R (eds) Computational plasticity. Computational methods in applied sciences, vol 7. Springer, Dordrecht, pp 87–103. https://doi.org/10.1007/978-1-4020-6577-4_6

60. Oñate E, Idelsohn SR, Del Pin F, Aubry R (2004) The particle finite element method—an overview. Int J Comput Methods 01(02):267–307

61. Oñate E, Idelsohn SR, Celigueta MA, Rossi R, Marti J, Carbonell JM, Ryzhakov P, Suárez B (2011) Advances in the particle finite element method (PFEM) for solving coupled problems in engineering. In: Oñate E, Owen R (eds) Particle-based methods, computational methods in applied sciences. Springer, Berlin

62. Pan B, Qian K, Xie H, Asundi A (2009) Two-dimensional digital image correlation for in-plane displacement and strain measurement: a review. Meas Sci Technol 20(6):062001

63. Peng C, Guo X, Wu W, Wang Y (2016) Unified modelling of granular media with smoothed particle hydrodynamics. Acta Geotech 11(6):1231–1247

64. Pestana JM, Whittle AJ (1999) Formulation of a unified constitutive model for clays and sands. Int J Numer Anal Methods Geomech 23(12):1215–1243

65. Pouliquen O, Cassar C, Jop P, Forterre Y, Nicolas M (2006) Flow of dense granular material: towards simple constitutive laws. J Stat Mech Theory Exp 2006(07):P07020

66. Radjai F, Richefeu V (2009) Contact dynamics as a nonsmooth discrete element method. Mech Mater 41(6):715–728

67. Rodríguez JM, Jonsén P, Svoboda A (2017) Simulation of metal cutting using the particle finite-element method and a physically based plasticity model. Comput Part Mech 4(1):35–51

68. Rodríguez JM, Carbonell JM, Jonsén P (2018) Numerical Methods for the modelling of chip formation. Arch Comput Methods Eng. https://doi.org/10.1007/s11831-018-09313-9

69. Saabye Ottosen N, Ristinmaa M (2005) The mechanics of constitutive modeling, 1st edn. Elsevier, Amsterdam

70. Salazar F, Irazábal J, Larese A, Oñate E (2016) Numerical modelling of landslide-generated waves with the particle finite element method (PFEM) and a non-Newtonian flow model. Int J Numer Anal Methods Geomech 40(6):809–826

71. Samiei K, Peters B, Bolten M, Frommer A (2013) Assessment of the potentials of implicit integration method in discrete element modelling of granular matter. Comput Chem Eng 49:183–193

72. Servin M, Wang D, Lacoursière C, Bodin K (2014) Examining the smooth and nonsmooth discrete element approaches to granular matter. Int J Numer Methods Eng 97(12):878–902

73. Sielamowicz I, Blonski S, Kowalewski TAA (2005) Optical technique DPIV in measurements of granular material flows, part 1 of 3—plane hoppers. Chem Eng Sci 60(2):589–598

74. Sołowski WT, Sloan SW (2015) Evaluation of material point method for use in geotechnics. Int J Numer Anal Methods Geomech 39(7):685–701

75. Sulsky D, Chen Z, Schreyer H (1994) A particle method for history-dependent materials. Comput Methods Appl Mech Eng 118(1–2):179–196

76. Sulsky D, Zhou SJ, Schreyer HL (1995) Application of a particle-in-cell method to solid mechanics. Comput Phys Commun 87(1–2):236–252

77. US Geological Survey (2010) Metals and minerals: U.S. Geological Survey Minerals Yearbook 2008, v. 1. U.S. Government Printing Office, Reston, Virginia, United States

78. Wang Y, Lu Y, Ooi JY (2013) Numerical modelling of dynamic pressure and flow in hopper discharge using the arbitrary Lagrangian–Eulerian formulation. Eng Struct 56:1308–1320

79. Warnett JM, Denissenko P, Thomas PJ, Kiraci E, Williams MA (2014) Scalings of axisymmetric granular column collapse. Granul Matter 16(1):115–124

80. Więckowski Z, Kowalska-Kubsik I (2011) Non-local approach in modelling of granular flow by the material point method. In: Proceedings of computer methods in mechanics, Warsaw, Poland, pp 101–102

81. Willert CE, Gharib M (1991) Digital particle image velocimetry. Exp Fluids 10(4):181–193

82. Wu CY, Cocks ACF (2006) Numerical and experimental investigations of the flow of powder into a confined space. Mech Mater 38(4):304–324

83. Wu YH, Hill JM, Yu A (2007) A finite element method for granular flow through a frictional boundary. Commun Nonlinear Sci Numer Simul 12(4):486–495

84. Xu X, Harada K (2003) Automatic surface reconstruction with alpha-shape method. Vis Comput 19(7–8):431–443

85. Xu X, Sun Q, Jin F, Chen Y (2016) Measurements of velocity and pressure of a collapsing granular pile. Powder Technol 303:147–155

86. Zhang X, Krabbenhoft K, Sheng D, Li W (2015) Numerical simulation of a flow-like landslide using the particle finite element method. Comput Mech 55(1):167–177

87. Zienkiewicz OC, Godbole PN (1974) Flow of plastic and visco-plastic solids with special reference to extrusion and forming processes. Int J Numer Methods Eng 8(1):1–16

88. Zienkiewicz OC, Taylor RL, Zhu JZ (2013) Finite element method: its basis and fundamentals, 7th edn. Butterworth-Heinemann, London